Available online at www.sciencedirect.com
ScienceDirect
Journal of Sound and Vibration 310 (2008) 1–20
JOURNAL OF SOUND AND VIBRATION
www.elsevier.com/locate/jsvi

Dynamic response of an elastic plate containing periodic masses

Andrew J. Hull*

Autonomous Systems and Technology Department, Naval Undersea Warfare Center Division, Newport, RI 02841, USA

Received 5 July 2005; received in revised form 4 December 2006; accepted 20 March 2007
Available online 7 November 2007

Abstract

This paper develops an analytical model that incorporates an infinite number of periodically spaced discrete masses into the equations of elasticity of a two-dimensional solid that is excited by a harmonic force in both time and space. Two specific problems are addressed. The first is that of a plate with the masses on the bottom edge, and the second is that of a plate with the masses embedded in the medium. The equations of elasticity are written as stress field expressions with the appropriate boundary conditions in the spatial-frequency domain. An infinite number of indexed equations are generated using an orthogonalization procedure. Once this is accomplished, all the indexed equations of the system are written together in a single matrix equation. The problem is then solved using a truncated set of terms and the displacement fields are transferred into the wavenumber–frequency domain for analysis. These results are compared to previously available low frequency model results for solutions involving the flexural wave in the plate. A numerical example is then solved at high frequency that includes higher-order wave motion, and this example is discussed.
Published by Elsevier Ltd.

1. Introduction

Plate theory has been researched extensively for many years. Early plate and beam theory [1] modeled displacement in thin plates and beams. These models contain primarily flexural wave dynamics and are inaccurate at high frequencies and wavenumbers. Rotary inertia and shear effects [2] were added to the flexural wave model to obtain more accurate results at increased frequencies. Fully elastic models [3] were developed to incorporate plate dynamics as the wavelengths of energy that propagate in the plate began to approach and surpass the thickness of the plate. Analysis has also been conducted on the dispersion curves of these systems, particularly in the area of free-wave propagation [4–9]. To a lesser extent, the mode shapes of these systems have been studied and documented [10,11].

The complexity of plate models has increased over the years by the addition of stiffeners (ribs) or masses. The problem of a fluid-loaded infinite thin plate with infinite sets of parallel stiffeners excited by a point load has been analyzed in a study that modeled the stiffeners as line forces [12]. This problem was extended to include a moment exerted by the stiffeners and forcing functions of plane wave, line, and point forces on beams [13] and plates [14,15]. The fluid-loaded infinite plate problem was reformulated for a finite number of equally spaced stiffeners [16] and was further studied for randomly spaced stiffeners [17]. The problem of a

*Tel.: +1 401 832 5189.
E-mail address: HullAJ@Npt.NUWC.Navy.Mil

0022-460X/$ - see front matter Published by Elsevier Ltd.
doi:10.1016/j.jsv.2007.03.085

fluid-loaded, aperiodic-stiffened infinite plate has also been addressed [18], as has the analysis of a finite-sized plate containing concentrated masses [19]. In these studies [12–19], the plate model has been either a thin plate or a thin plate with rotary inertia and shear effects. Finally, the problem was modeled using finite elements to produce numerical solutions [20]. It is noted that the modeling technique of adding a stiffener to the plate is similar to that of adding a discrete mass to the plate.

This paper presents an analytical model that incorporates an infinite number of periodically spaced masses into the equations of elasticity that model motion and stress in a two-dimensional fully elastic solid. This model is intended to be used for high frequency analysis where a relatively soft medium contains embedded pieces that have much higher density, e.g. coated structures that for various reasons have to contain heavier pieces. The formulation of the problem begins with elasticity theory, that models the motion in the solid as a combination of dilatational and shear waves. From this theory, an expression for plate displacement is obtained. The displacements are then inserted into stress relationships that are set equal to the forces acting on the structure by the masses. The problem is then written as a dynamic system, in matrix form, where the left-hand terms represent the zero-order mode and is equal to an infinite number of right-hand terms that represent the masses acting on the structure plus a term that models the plane wave forcing function. Rewriting this zero-order term by increasing and decreasing the mode index results in an expression for the higher-order modes. The integer shift property is then applied to the right-hand side of all of the terms, resulting in an infinite set of equations that model the wave propagation coefficients of all the modes of the structure. This set of equations is truncated to a finite number of terms, and a solution to the displacement and stress field is calculated. Two different cases are examined: (1) where the masses are on the edge of the plate and (2) where the masses reside within the interior of the plate. The solution is compared to a previously solved problem at low frequency where the wavelength of the harmonic forcing function is large compared to the thickness of the plate. A numerical example of a high-frequency problem is included and discussed.

2. Elastic plate with masses aligned on the lower surface

The first problem analyzed is that of an elastic plate with discrete (point) masses at the bottom edge, as shown in Fig. 1. The masses on the bottom of the plate are equally spaced a distance of L (m) in the x-direction and each has a mass per unit length of M (kg/m). The plate has a thickness of h (m) and is loaded on the top surface with a normal forcing function. The model is based on the following assumptions: (1) the forcing function acting on the plate is a plane wave at a definite wavenumber and frequency, (2) the corresponding response of the plate is at definite periodic wavenumbers and definite frequency, (3) motion is normal and tangential to the plate in one direction (two-dimensional system), (4) the plate has infinite spatial extent in the x-direction, (5) the masses have translational degrees of freedom in the x- and z-directions, and (6) the particle motion is linear.

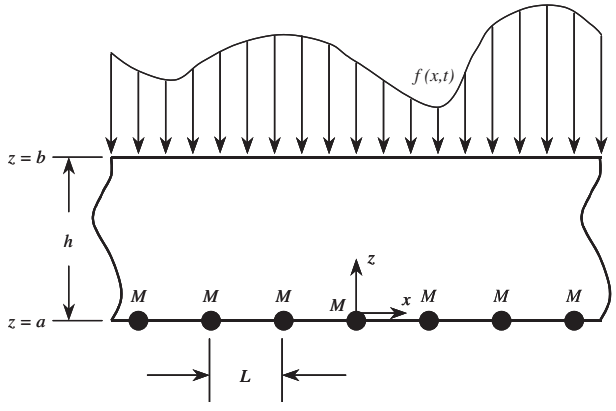

Fig. 1. Elastic plate with periodic edge masses.

The motion of the elastic plate is governed by the equation [21]

$$\mu\nabla^2\mathbf{g}(x,y,z,t)+(\lambda+\mu)\nabla\nabla\cdot\mathbf{g}(x,y,z,t)=\rho\frac{\partial^2\mathbf{g}(x,y,z,t)}{\partial t^2}, \tag{1}$$

where ρ is the density (kg/m^3), λ and μ are the Lamé constants (N/m^2), t is time (s), $\cdot$ denotes a vector dot product, and $\mathbf{g}(x,y,z,t)$ is the three-dimensional Cartesian coordinate displacement vector and is written as

$$\mathbf{g}(x,y,z,t)=\begin{Bmatrix}u(x,y,z,t)\\v(x,y,z,t)\\w(x,y,z,t)\end{Bmatrix}=\nabla\phi(x,y,z,t)+\nabla\times\begin{Bmatrix}\psi_x(x,y,z,t)\\\psi_y(x,y,z,t)\\\psi_z(x,y,z,t)\end{Bmatrix}, \tag{2}$$

where ϕ is a dilatational scalar potential, ∇ is the gradient operator, $\times$ denotes a vector crossproduct, and $\vec{\psi}$ is an equivoluminal vector potential. The formulation is now condensed into a two-dimensional problem; thus, $v\equiv 0$ and $\partial(\cdot)/\partial y\equiv 0$. Expanding Eq. (2) and breaking the displacement vector into its individual nonzero terms yields

$$u(x,z,t)=\frac{\partial\phi(x,z,t)}{\partial x}-\frac{\partial\psi_y(x,z,t)}{\partial z}, \tag{3}$$

and

$$w(x,z,t)=\frac{\partial\phi(x,z,t)}{\partial z}+\frac{\partial\psi_y(x,z,t)}{\partial x}, \tag{4}$$

where $u(x,z,t)$ is the displacement field (m) in the tangential (horizontal) direction and $w(x,z,t)$ is the displacement field in the normal (vertical) direction (m). Eqs. (3) and (4) are next inserted into Eq. (1), which results in two decoupled wave equations, given by

$$c_d^2\nabla^2\phi(x,z,t)=\frac{\partial^2\phi(x,z,t)}{\partial t^2}, \tag{5}$$

and

$$c_s^2\nabla^2\psi_y(x,z,t)=\frac{\partial^2\psi_y(x,z,t)}{\partial t^2}, \tag{6}$$

where Eq. (5) corresponds to the dilatational component and Eq. (6) corresponds to the shear component of the displacement field. Correspondingly, the constants c_d and c_s are the complex dilatational and shear wave speeds, respectively, and are determined by

$$c_d=\sqrt{\frac{\lambda+2\mu}{\rho}}, \tag{7}$$

and

$$c_s=\sqrt{\frac{\mu}{\rho}}. \tag{8}$$

The displacement field is modeled as a sum of functions with respect to spatial coordinate z multiplied by an exponential in space and time. Using this form, Eqs. (5) and (6) can be solved separately. The result is then inserted into Eqs. (3) and (4), and noting as others have [13] that the response is spatially harmonic for

spatially periodic systems, gives the individual displacement fields as

$$u(x,z,t) = \sum_{m=-\infty}^{m=+\infty} U_m(z)\,\exp(\mathrm{i}k_m x)\exp(-\mathrm{i}\omega t)$$
$$= \sum_{m=-\infty}^{m=+\infty} [A_m \mathrm{i}k_m\,\sin(\alpha_m z) + B_m \mathrm{i}k_m\,\cos(\alpha_m z)$$
$$- C_m\beta_m\,\cos(\beta_m z) + D_m\beta_m\,\sin(\beta_m z)]\exp(\mathrm{i}k_m x)\exp(-\mathrm{i}\omega t), \quad (9a, b)$$

and

$$w(x,z,t) = \sum_{m=-\infty}^{m=+\infty} W_m(z)\exp(\mathrm{i}k_m x)\exp(-\mathrm{i}\omega t)$$
$$= \sum_{m=-\infty}^{m=+\infty} [A_m\alpha_m\,\cos(\alpha_m z) - B_m\alpha_m\,\sin(\alpha_m z)$$
$$+ C_m \mathrm{i}k_m\,\sin(\beta_m z) + D_m \mathrm{i}k_m\,\cos(\beta_m z)]\exp(\mathrm{i}k_m x)\exp(-\mathrm{i}\omega t), \quad (10a, b)$$

where A_m, B_m, C_m, and D_m are complex wave propagation coefficients of the plate and are determined by solving the system of equations below using four boundary conditions: $\mathrm{i} = \sqrt{-1}$, ω is the frequency (rad/s), k_m is the spatial periodic wavenumber (rad/m) and is written as

$$k_m = k + \frac{2\pi m}{L}, \quad (11)$$

where k is the wavenumber (rad/m) with respect to the x axis, α_m is the modified wavenumber (rad/m) associated with the dilatational wave and is expressed as

$$\alpha_m = \sqrt{k_d^2 - k_m^2}, \quad (12)$$

where k_d is the dilatational wavenumber and is equal to ω/c_d, with c_d being the dilatational wavespeed (m/s); β_m is the modified wavenumber (rad/m) associated with the shear wave and is expressed as

$$\beta_m = \sqrt{k_s^2 - k_m^2}, \quad (13)$$

where k_s is the shear wavenumber (rad/m) equal to ω/c_s and c_s is the shear wavespeed (m/s). To solve for the wave propagation coefficients, the boundary conditions at the top and bottom of the plate have to be specified.

If the plate edges contain only the normal forcing function shown in Fig. 1 (i.e. the masses are absent), the normal stress on the top of the plate ($z = b$) is

$$\tau_{zz}(x,b,t) = (\lambda + 2\mu)\frac{\partial u_z(x,b,t)}{\partial z} + \lambda\frac{\partial u_x(x,b,t)}{\partial x} = -f(x,t), \quad (14)$$

the tangential stress on the top of the plate is

$$\tau_{zx}(x,b,t) = \mu\left[\frac{\partial u_x(x,b,t)}{\partial z} + \frac{\partial u_z(x,b,t)}{\partial x}\right] = 0, \quad (15)$$

the normal stress on the bottom of the plate ($z = a$) is

$$\tau_{zz}(x,a,t) = (\lambda + 2\mu)\frac{\partial u_z(x,a,t)}{\partial z} + \lambda\frac{\partial u_x(x,a,t)}{\partial x} = 0, \quad (16)$$

and the tangential stress on the bottom of the plate is

$$\tau_{zx}(x,a,t) = \mu\left[\frac{\partial u_x(x,a,t)}{\partial z} + \frac{\partial u_z(x,a,t)}{\partial x}\right] = 0, \quad (17)$$

where $f(x,t)$ is the forcing function exciting the top of the plate expressed in force per unit area ($\mathrm{N/m^2}$). Eqs. (1) and (14)–(17) are the governing partial differential equations and the boundary conditions for the

displacement in an elastic plate excited by a continuous forcing function on one edge or boundary. For a harmonic space–time loaded structure, the forcing function is given as

$$f(x,t) = F\ \exp(\mathrm{i}kx)\exp(-\mathrm{i}\omega t). \tag{18}$$

This is a traditional boundary value problem that is formulated and solved in many classical textbooks. The problem of interest in this paper, however, is the discrete mass loading, and these dynamic forces are now added to the boundary conditions when they reside on the bottom edge.

The normal stress due to the forces induced by the motion of the masses is equal to the summation of the mass multiplied by the acceleration in the z-direction times the spatial Dirac delta function for each individual mass. This expression is

$$\tau_{zz}(x,a,t) = \sum_{n=-\infty}^{n=+\infty} M\frac{\partial^2 u_z(x,a,t)}{\partial t^2}\delta(x-nL). \tag{19}$$

Similarly, the tangential stress due to the forces induced by the motion of the masses is equal to the summation of the mass multiplied by the acceleration in the x-direction times the spatial Dirac delta function for each individual mass. This equation is written as

$$\tau_{zx}(x,a,t) = \sum_{n=-\infty}^{n=+\infty} M\frac{\partial^2 u_x(x,a,t)}{\partial t^2}\delta(x-nL). \tag{20}$$

It is noted that each mass can also be attached to ground with a parallel spring and damper by replacing the mass times vertical acceleration term

$$M\frac{\partial^2 u_z(x,a,t)}{\partial t^2} \tag{21}$$

with

$$M\frac{\partial^2 u_z(x,a,t)}{\partial t^2} + P\frac{\partial u_z(x,a,t)}{\partial t} + Ku_z(x,a,t), \tag{22}$$

where in Eq. (22), P is the viscous damping coefficient per unit length ($\mathrm{N\,s/m^2}$), and K is the spring constant per unit length ($\mathrm{N/m^2}$). This system, shown in Fig. 2, corresponds to a periodically damped and stiffened elastic plate with discrete masses.

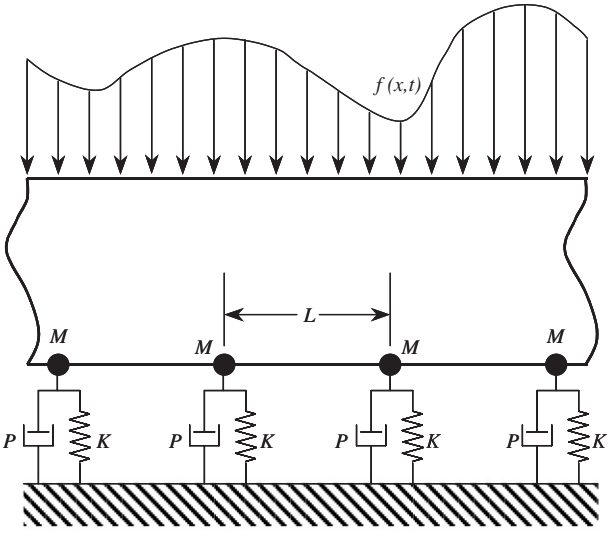

Fig. 2. Elastic plate with periodic edge masses, dampers, and springs.

The equations for the wave propagation coefficients are obtained by inserting Eqs. (9a) and (10a) into Eqs. (14)–(17) along with the mass boundary conditions given by Eqs. (19) and (20) and the forcing function in Eq. (18). This yields

$$(\lambda+2\mu)\sum_{m=-\infty}^{m=+\infty}\frac{\partial W_m(b)}{\partial z}\exp(\mathrm{i}k_m x)+\mathrm{i}k_m\lambda\sum_{m=-\infty}^{m=+\infty}U_m(b)\exp(\mathrm{i}k_m x)=-F\exp(\mathrm{i}kx), \tag{23}$$

$$\mu\left[\sum_{m=-\infty}^{m=+\infty}\frac{\partial U_m(b)}{\partial z}\exp(\mathrm{i}k_m x)+\mathrm{i}k_m\sum_{m=-\infty}^{m=+\infty}W_m(b)\exp(\mathrm{i}k_m x)\right]=0, \tag{24}$$

$$\begin{aligned}&(\lambda+2\mu)\sum_{m=-\infty}^{m=+\infty}\frac{\partial W_m(a)}{\partial z}\exp(\mathrm{i}k_m x)+\mathrm{i}k_m\lambda\sum_{m=-\infty}^{m=+\infty}U_m(a)\exp(\mathrm{i}k_m x)\\&\quad=-\omega^2 M\sum_{n=-\infty}^{n=+\infty}\left[\sum_{m=-\infty}^{m=+\infty}W_m(a)\exp(\mathrm{i}k_m x)\right]\delta(x-nL),\end{aligned} \tag{25}$$

and

$$\begin{aligned}&\mu\left[\sum_{m=-\infty}^{m=+\infty}\frac{\partial U_m(a)}{\partial z}\exp(\mathrm{i}k_m x)+\mathrm{i}k_m\sum_{m=-\infty}^{m=+\infty}W_m(a)\exp(\mathrm{i}k_m x)\right]\\&\quad=-\omega^2 M\sum_{n=-\infty}^{n=+\infty}\left[\sum_{m=-\infty}^{m=+\infty}U_m(a)\exp(\mathrm{i}k_m x)\right]\delta(x-nL).\end{aligned} \tag{26}$$

The Dirac delta comb function that is present in Eqs. (25) and (26) obeys the relationship

$$\sum_{n=-\infty}^{n=+\infty}\delta(x-nL)=\frac{1}{L}\sum_{n=-\infty}^{n=+\infty}\exp(\mathrm{i}2\pi nx/L), \tag{27}$$

and using this equation, Eqs. (25) and (26) become

$$\begin{aligned}&(\lambda+2\mu)\sum_{m=-\infty}^{m=+\infty}\frac{\partial W_m(a)}{\partial z}\exp(\mathrm{i}k_m x)+\mathrm{i}k_m\lambda\sum_{m=-\infty}^{m=+\infty}U_m(a)\exp(\mathrm{i}k_m x)\\&\quad=\frac{-\omega^2 M}{L}\sum_{n=-\infty}^{n=+\infty}\left[\sum_{m=-\infty}^{m=+\infty}W_m(a)\exp(\mathrm{i}k_m x)\right]\exp(\mathrm{i}2\pi nx/L),\end{aligned} \tag{28}$$

and

$$\begin{aligned}&\mu\left[\sum_{m=-\infty}^{m=+\infty}\frac{\partial U_m(a)}{\partial z}\exp(\mathrm{i}k_m x)+\mathrm{i}k_m\sum_{m=-\infty}^{m=+\infty}W_m(a)\exp(\mathrm{i}k_m x)\right]\\&\quad=\frac{-\omega^2 M}{L}\sum_{n=-\infty}^{n=+\infty}\left[\sum_{m=-\infty}^{m=+\infty}U_m(a)\exp(\mathrm{i}k_m x)\right]\exp(\mathrm{i}2\pi nx/L).\end{aligned} \tag{29}$$

Both the n and m summations run from minus infinity to plus infinity, therefore, the following relationship must hold true:

$$\sum_{n=-\infty}^{n=+\infty}\left[\sum_{m=-\infty}^{m=+\infty}W_m(a)\exp(\mathrm{i}k_m x)\right]\exp(\mathrm{i}2\pi nx/L)=\left[\sum_{n=-\infty}^{n=+\infty}W_n(a)\right]\sum_{m=-\infty}^{m=+\infty}\exp(\mathrm{i}k_m x). \tag{30}$$

Eq. (30) is also applicable to the $U_m(a)$ term, and inserting this into Eqs. (28) and (29) yields

$$(\lambda+2\mu)\sum_{m=-\infty}^{m=+\infty}\frac{\partial W_m(a)}{\partial z}\exp(\mathrm{i}k_m x)+\mathrm{i}k_m\lambda\sum_{m=-\infty}^{m=+\infty}U_m(a)\exp(\mathrm{i}k_m x)$$
$$=\frac{-\omega^2 M}{L}\left[\sum_{n=-\infty}^{n=+\infty}W_n(a)\right]\sum_{m=-\infty}^{m=+\infty}\exp(\mathrm{i}k_m x), \tag{31}$$

and

$$\mu\left[\sum_{m=-\infty}^{m=+\infty}\frac{\partial U_m(a)}{\partial z}\exp(\mathrm{i}k_m x)+\mathrm{i}k_m\sum_{m=-\infty}^{m=+\infty}W_m(a)\exp(\mathrm{i}k_m x)\right]$$
$$=\frac{-\omega^2 M}{L}\left[\sum_{n=-\infty}^{n=+\infty}U_n(a)\right]\sum_{m=-\infty}^{m=+\infty}\exp(\mathrm{i}k_m x). \tag{32}$$

Eqs. (23), (24), (31), and (32) are now all multiplied by $\exp(-\mathrm{i}k_p x)$ and integrated from $[0,L]$. This results in an orthogonal relationship, and the series terms of the equations will decouple into individual m indexed equations. The normal stress equation at $z=b$ becomes

$$(\lambda+2\mu)\frac{\partial W_m(b)}{\partial z}+\mathrm{i}k_m\lambda U_m(b)=\begin{cases}-F, & m=0,\\ 0, & m\neq 0,\end{cases} \tag{33}$$

and the tangential stress equation at $z=b$ becomes

$$\mu\left[\frac{\partial U_m(b)}{\partial z}+\mathrm{i}k_m W_m(b)\right]=0. \tag{34}$$

The normal stress equation at $z=a$ becomes

$$(\lambda+2\mu)\frac{\partial W_m(a)}{\partial z}+\mathrm{i}k_m\lambda U_m(a)=\frac{-M\omega^2}{L}\sum_{n=-\infty}^{n=+\infty}W_n(a), \tag{35}$$

and the tangential stress equation at $z=a$ becomes

$$\mu\left[\frac{\partial U_m(a)}{\partial z}+\mathrm{i}k_m W_m(a)\right]=\frac{-M\omega^2}{L}\sum_{n=-\infty}^{n=+\infty}U_n(a). \tag{36}$$

Eqs. (9b) and (10b) are inserted into Eqs. (33)–(36); however, this substitution alone does not produce a solution to the problem, because the result is four equations and an infinite number of unknowns. This substitution for $m=0$ is rewritten in matrix form as

$$[\mathbf{A}^{(0)}(k)]\{\mathbf{x}^{(0)}(k)\}=\sum_{n=-\infty}^{n=+\infty}[\mathbf{U}^{(n)}(k_n)]\{\mathbf{x}^{(n)}(k_n)\}+\mathbf{f}, \tag{37}$$

where $[\mathbf{A}^{(0)}(k)]$ is a four by four matrix that models the dynamics of the plate for $m=0$, $\{\mathbf{x}^{(0)}(k)\}$ is the four by one vector of wave propagation coefficients for $m=0$, $[\mathbf{U}^{(n)}(k_n)]$ is the four by four matrix that represents the periodic mass loading on the structure for nth mode, $\{\mathbf{x}^{(n)}(k_n)\}$ is the four by one vector of wave propagation coefficients for nth mode, and $\mathbf{f}$ is the four by one vector that models the plane wave excitation. The entries of the matrices and vectors in Eq. (37) are listed in Appendix A. It is noted that in the absence of masses, all $[\mathbf{U}^{(n)}(k_n)]$ terms are zero, and Eq. (37) regresses into the traditional elastic plate problem given in Eqs. (14)–(17).

To facilitate a solution to the problem, index shifting is employed. The integer shift property of an infinite summation is applied to Eq. (37), which results in

$$[\mathbf{A}^{(m)}(k_m)]\{\mathbf{x}^{(m)}(k_m)\} = \sum_{n=-\infty}^{n=+\infty} [\mathbf{U}^{(n+m)}(k_{(n+m)})]\{\mathbf{x}^{(n+m)}(k_{(n+m)})\} + \begin{cases} \mathbf{f}, & m=0 \\ \mathbf{0}, & m\neq 0 \end{cases}$$
$$= \sum_{n=-\infty}^{n=+\infty} [\mathbf{U}^{(n)}(k_n)]\{\mathbf{x}^{(n)}(k_n)\} + \begin{cases} \mathbf{f}, & m=0, \\ \mathbf{0}, & m\neq 0, \end{cases} \tag{38}$$

where the $\mathbf{0}$ term is a four by one vector whose entries are all zeros. Once the $[\mathbf{A}^{(m)}]$ matrix is integer-indexed and the displacement load matrix indices have been shifted, the system equations can be rewritten using all the n-indexed modes as

$$\mathbf{A}\,\mathbf{x} = \mathbf{U}\,\mathbf{x} + \mathbf{F}, \tag{39}$$

where $\mathbf{A}$ is a block-diagonal matrix and is equal to

$$\mathbf{A} = \begin{bmatrix} \ddots & & \vdots & & \iddots \\ & [\mathbf{A}^{(-1)}(k_{-1})] & \mathbf{0} & \mathbf{0} & \\ \cdots & \mathbf{0} & [\mathbf{A}^{(0)}(k)] & \mathbf{0} & \cdots \\ & \mathbf{0} & \mathbf{0} & [\mathbf{A}^{(1)}(k_1)] & \\ \iddots & & \vdots & & \ddots \end{bmatrix}, \tag{40}$$

$\mathbf{U}$ is a rank deficient, block-partitioned matrix and is written as

$$\mathbf{U} = \begin{bmatrix} \ddots & & \vdots & & \iddots \\ & [\mathbf{U}^{(-1)}(k_{-1})] & [\mathbf{U}^{(0)}(k)] & [\mathbf{U}^{(1)}(k_1)] & \\ \cdots & [\mathbf{U}^{(-1)}(k_{-1})] & [\mathbf{U}^{(0)}(k)] & [\mathbf{U}^{(1)}(k_1)] & \cdots \\ & [\mathbf{U}^{(-1)}(k_{-1})] & [\mathbf{U}^{(0)}(k)] & [\mathbf{U}^{(1)}(k_1)] & \\ \iddots & & \vdots & & \ddots \end{bmatrix}, \tag{41}$$

$\mathbf{F}$ is the plane wave load vector

$$\mathbf{F} = [\cdots \quad \mathbf{0}^{\mathrm{T}} \quad \mathbf{f}^{\mathrm{T}} \quad \mathbf{0}^{\mathrm{T}} \quad \cdots]^{\mathrm{T}}, \tag{42}$$

and $\mathbf{x}$ is the wave propagation coefficient vector that contains all the unknown indexed coefficients as

$$\mathbf{x} = [\cdots \quad \{\mathbf{x}^{(-1)}(k_{-1})\}^{\mathrm{T}} \quad \{\mathbf{x}^{(0)}(k)\}^{\mathrm{T}} \quad \{\mathbf{x}^{(1)}(k_1)\}^{\mathrm{T}} \quad \cdots]^{\mathrm{T}}. \tag{43}$$

The $\mathbf{0}$ term in Eq. (40) is a four by four matrix whose entries are all zeros and the $\mathbf{0}$ term in Eq. (42) is a four by one vector whose entries are all zeros. Eq. (39) is assembled, and the wave-propagation coefficients that reside in the $\mathbf{x}$ vector can be determined using

$$\mathbf{x} = [\mathbf{A} - \mathbf{U}]^{-1}\mathbf{F}. \tag{44}$$

When the coefficients are determined, the displacements of the system in the spatial domain can be calculated using Eqs. (9b) and (10b).

For many analytical problems, it is desirable to transform the solution into the wavenumber–frequency domain for analysis. For a function that is periodic on the interval $[0,L]$, the Fourier transform into the wavenumber domain is

$$\hat{\mathbf{G}}(k) = \frac{1}{L}\int_0^L \mathbf{g}(x,z,t)\exp(-\mathrm{i}kx)\,\mathrm{d}x. \tag{45}$$

Insertion of Eqs. (9b) and (10b) into Eq. (45) results in the integrand for all the $n\neq 0$ terms equaling zero, and this results in

$$\hat{u}(k,z,t) = [A_0\mathrm{i}k\,\sin(\alpha_0 z) + B_0\mathrm{i}k\,\cos(\alpha_0 z) - C_0\beta_0\,\cos(\beta_0 z) + D_0\beta_0\,\sin(\beta_0 z)]\exp(-\mathrm{i}\omega t), \tag{46}$$

and

$$\hat{w}(k,z,t) = [A_0\alpha_0\cos(\alpha_0 z) - B_0\alpha_0\sin(\alpha_0 z) + C_0 ik\sin(\beta_0 z) + D_0 ik\cos(\beta_0 z)]\exp(-i\omega t), \tag{47}$$

where the hat overscript denotes the displacement function in the wavenumber domain.

The elastic plate model can be compared and, thus, validated for a relatively thin plate at low frequency using the Timoshenko–Mindlin differential equation of motion applied to an infinite plate containing periodic masses. This model has been previously analyzed [12,19] using a line load excitation and the Bernoulli–Euler differential equation of motion. This model has one degree of freedom that is the displacement in the z-direction. It is reformulated below to correspond to plane wave excitation and to include shear and rotary inertia effects of the plate. This transfer function of normal displacement divided by excitation force is

$$\frac{\hat{w}(k,\omega)}{F} = T(k)\left[\frac{1-(M\omega^2/L)T(k)+(M\omega^2/L)\sum_{n=-\infty}^{n=+\infty}T(k_n)}{1+(M\omega^2/L)\sum_{n=-\infty}^{n=+\infty}T(k_n)}\right]\exp(-i\omega t), \tag{48}$$

where

$$T(k) = \frac{-1-(D/\kappa^2\mu h)k^2+(\rho h^2/12\kappa^2\mu)\omega^2}{Dk^4-[(D\rho/\kappa^2\mu)+(\rho h^3/12)]\omega^2k^2+(\rho^2h^3/12\kappa^2\mu)\omega^4-(\rho h)\omega^2}, \tag{49}$$

$$D = \frac{Eh^3}{12(1-\upsilon^2)}, \tag{50}$$

and

$$\kappa^2 = \frac{5}{6-\upsilon}. \tag{51}$$

In Eqs. (49) and (50), E is Young's modulus (N/m^2) and υ is Poisson's ratio (dimensionless).

Fig. 3 is a plot of the transfer function of displacement in the z-direction divided by input force versus wavenumber at a frequency of 220 Hz. The time exponential function has been suppressed. This example was generated with the following system parameters: thickness is 0.01 m, density is 1200 kg/m^3, Lamé constant λ is 2.25×10^8 N/m^2, and Lamé constant μ is 2.50×10^7 N/m^2. In Fig. 3, the dashed line is Timoshenko–Mindlin plate theory without the periodic masses (i.e., $M=0$); the solid line is elastic plate theory with $M=0.5$ kg/m and $L=0.2$ m and corresponds to Eq. (47); and the x symbols are Timoshenko–Mindlin plate theory with $M=0.5$ kg/m and $L=0.2$ m and corresponds to Eq. (48). The elastic plate model was calculated using seven modes ($-3\leqslant n\leqslant 3$) that produced a 28-by 28-element system matrix. The resonance exhibited by the Timoshenko–Mindlin plate model is the plate flexural wave. This energy is shifted higher in wavenumber as masses are added to the system. Additionally, the added masses facilitate wave propagation in the system at integer multiples of the characteristic lengths of the mass separation distance. These effects, frequently called Floquet waves, can be seen at around 13, 15 and 50 rad/m. The transfer function in the x-direction is not shown because the Timoshenko–Mindlin equation of motion does not support a degree of freedom in this longitudinal direction.

Fig. 4 is a plot of the elastic plate transfer function calculated using one, three, five, and seven terms compared to Timoshenko–Mindlin plate theory for the above example. This plot illustrates the behavior of the model as more terms are added to the truncated model. Notice that more terms, in general, correspond to dynamics at higher wavenumbers. Numerical simulations suggest that every indexed (nontruncated) term retained in the analysis corresponds to a resonant peak in the response. The convergence of three, five, and seven term fully elastic models to the Timoshenko–Mindlin model was demonstrated by comparing the average difference in normal displacement magnitude values. For this convergence test, the frequency was changed to 50 Hz and the wavenumber range of 0 to 60 rad/m was retained. These low values of frequency and wavenumber insured that the Timoshenko–Mindlin model was evaluated in a region where the models' assumptions are valid. The average difference between the two models was 0.0076 for the three term elastic model, 0.0064 for the five term elastic model, and 0.0069 for the seven term elastic model. This comparison shows analytical convergence between the two models.

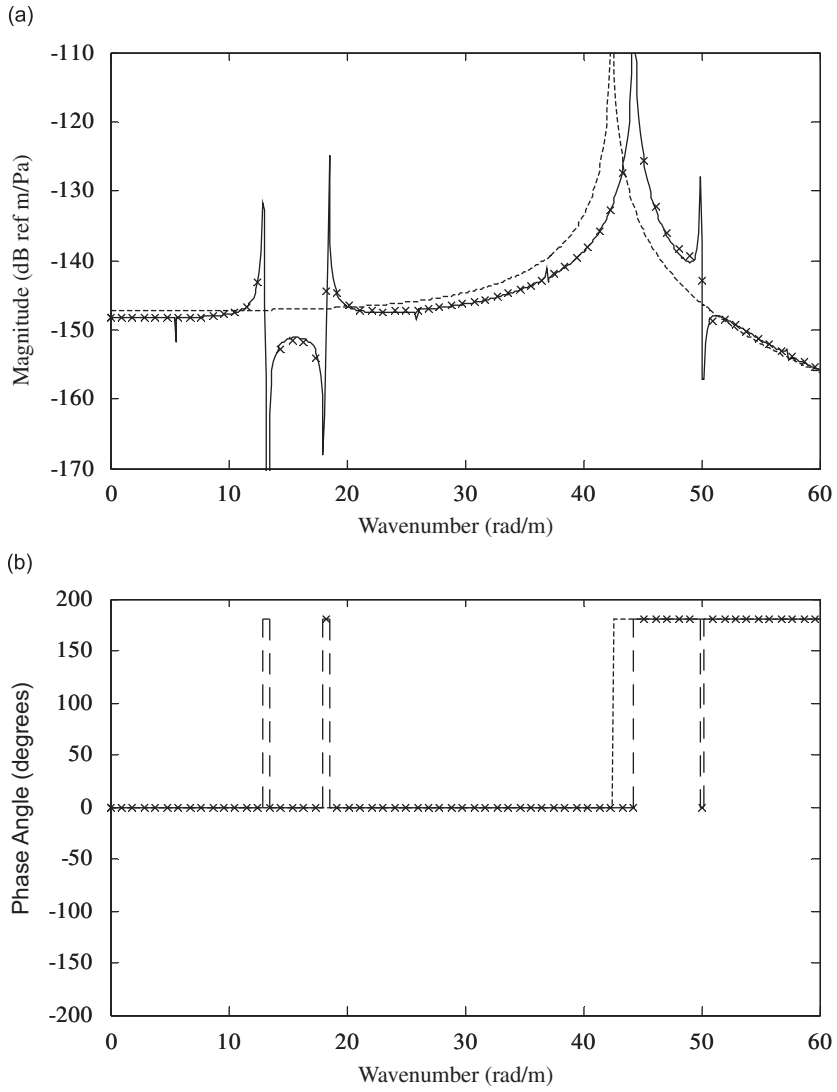

Fig. 3. Transfer function of displacement divided by excitation force versus wavenumber at 220 Hz: (a) magnitude and (b) phase angle. (------) Timoshenko–Mindlin plate, no added masses; (_____) elastic plate, added masses; and (x) Timoshenko–Mindlin plate, added masses.

3. Elastic plate with embedded interior masses

The elastic plate model can be modified so that the periodic masses are moved from the edge into the interior of the plate, as shown in Fig. 5. The solution to this problem is divided into two domains based on the value of z. The upper region of the plate, location $b \leqslant z \leqslant c$, is denoted with a prefix superscript (2), and the lower region of the plate, location $a \leqslant z \leqslant b$, is denoted with a prefix superscript (1). The displacement in the x-direction, which is found by applying Eq. (9) on two different regions, is

$$u(x,z,t) = \begin{cases} \sum_{m=-\infty}^{m=+\infty} [^{(2)}U_m(z)] \exp(\mathrm{i}k_m x) \exp(-\mathrm{i}\omega t), & b \leqslant z \leqslant c, \\ \sum_{m=-\infty}^{m=+\infty} [^{(1)}U_m(z)] \exp(\mathrm{i}k_m x) \exp(-\mathrm{i}\omega t), & a \leqslant z \leqslant b, \end{cases} \tag{52}$$

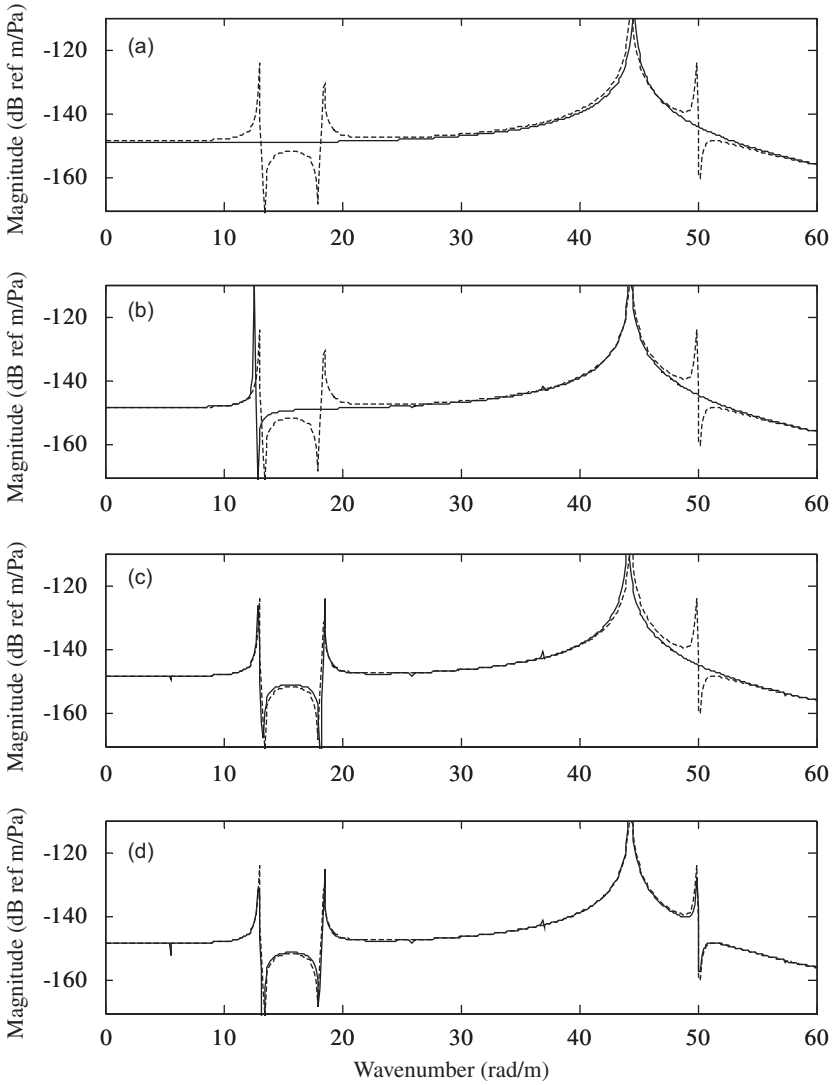

Fig. 4. Comparison of transfer functions, (____) elastic plate and (------) Timoshenko–Mindlin plate: (a) one elastic plate term, (b) three elastic plate terms, (c) five elastic plate terms, and (d) seven elastic plate terms.

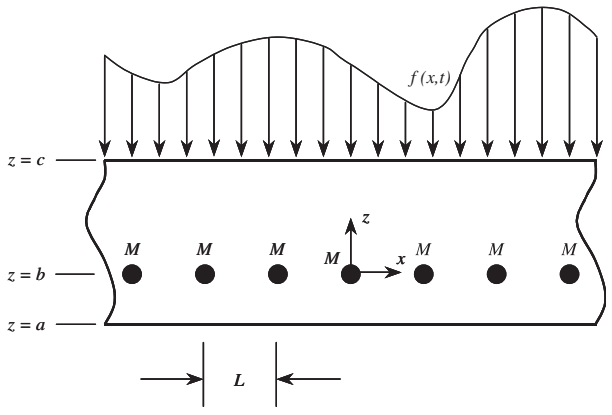

Fig. 5. Elastic plate with periodic interior masses.

where

$$^{(2)}U_m(z) = A_m \mathrm{i}k_m \sin(\alpha_m z) + B_m \mathrm{i}k_m \cos(\alpha_m z) - C_m \beta_m \cos(\beta_m z) + D_m \beta_m \sin(\beta_m z), \tag{53}$$

and

$$^{(1)}U_m(z) = E_m \mathrm{i}k_m \sin(\alpha_m z) + F_m \mathrm{i}k_m \cos(\alpha_m z) - G_m \beta_m \cos(\beta_m z) + H_m \beta_m \sin(\beta_m z). \tag{54}$$

Similarly, the displacement in the z-direction is

$$w(x,z,t) = \begin{cases} \sum_{m=-\infty}^{m=+\infty} [^{(2)}W_m(z)] \exp(\mathrm{i}k_m x) \exp(-\mathrm{i}\omega t), & b \leqslant z \leqslant c, \\ \sum_{m=-\infty}^{m=+\infty} [^{(1)}W_m(z)] \exp(\mathrm{i}k_m x) \exp(-\mathrm{i}\omega t), & a \leqslant z \leqslant b, \end{cases} \tag{55}$$

where

$$^{(2)}W_m(z) = A_m \alpha_m \cos(\alpha_m z) - B_m \alpha_m \sin(\alpha_m z) + C_m \mathrm{i}k_m \sin(\beta_m z) + D_m \mathrm{i}k_m \cos(\beta_m z), \tag{56}$$

and

$$^{(1)}W_m(z) = E_m \alpha_m \cos(\alpha_m z) - F_m \alpha_m \sin(\alpha_m z) + G_m \mathrm{i}k_m \sin(\beta_m z) + H_m \mathrm{i}k_m \cos(\beta_m z). \tag{57}$$

There are eight boundary conditions that govern the system; two at the top, four at the interface between region one and two, and two at the bottom. The first two equations are the normal and tangential stress, respectively, at the top surface of the upper plate:

$$^{(2)}\tau_{zz}(x,c,t) = -f(x,t), \tag{58}$$

and

$$^{(2)}\tau_{zx}(x,c,t) = 0. \tag{59}$$

The next four boundary conditions are the interface equations on the plane where the masses reside. The normal and tangential stress balances, respectively, between the upper and lower region of the plate, can be calculated using Eqs. (16), (17), (19), and (20) evaluated at $z = b$. They are

$$^{(2)}\tau_{zz}(x,b,t) - {}^{(1)}\tau_{zz}(x,b,t) = \sum_{n=-\infty}^{n=+\infty} M \frac{\partial^2 u_z(x,b,t)}{\partial t^2} \delta(x - nL), \tag{60}$$

and

$$^{(2)}\tau_{zx}(x,b,t) - {}^{(1)}\tau_{zx}(x,b,t) = \sum_{n=-\infty}^{n=+\infty} M \frac{\partial^2 u_x(x,b,t)}{\partial t^2} \delta(x - nL). \tag{61}$$

Continuity of displacement in the z- and x-directions at the interface are

$$^{(2)}w(x,b,t) - {}^{(1)}w(x,b,t) = 0, \tag{62}$$

and

$$^{(2)}u(x,b,t) - {}^{(1)}u(x,b,t) = 0. \tag{63}$$

The final two boundary conditions are the normal and tangential stress at the bottom surface of the lower plate:

$$^{(1)}\tau_{zz}(x,a,t) = 0, \tag{64}$$

and

$$^{(1)}\tau_{zx}(x,a,t) = 0. \tag{65}$$

Eqs. (52)–(57) are now substituted into Eqs. (58)–(65) and the orthogonalization procedure developed in Section 2 is applied to these equations yielding

$$[\mathbf{B}^{(0)}(k)]\{\mathbf{y}^{(0)}(k)\} = \sum_{n=-\infty}^{n=+\infty} [\mathbf{V}^{(n)}(k_n)]\{\mathbf{y}^{(n)}(k_n)\} + \mathbf{h}, \tag{66}$$

where $[\mathbf{B}^{(0)}(k)]$ is an eight by eight matrix that models the dynamics of the plate for $m = 0$, $\{\mathbf{y}^{(0)}(k)\}$ is the eight by one vector of wave propagation coefficients for $m = 0$, $[\mathbf{V}^{(n)}(k_n)]$ is the eight by eight matrix that represents the periodic mass loading on the structure for the nth mode, $\{\mathbf{y}^{(n)}(k_n)\}$ is the eight by one vector of wave propagation coefficients for the nth mode, and $\mathbf{h}$ is the eight by one vector that models the plane wave excitation. The matrix and vector entries in Eq. (66) are listed in Appendix A. The solution method is identical to that shown in the previous section for the plate with edge masses, although each n-indexed vector has eight entries associated with it instead of the four entries when the masses are on the edge of the plate. Thus, the solution becomes

$$\mathbf{y} = [\mathbf{B} - \mathbf{V}]^{-1}\mathbf{H}. \tag{67}$$

The previous example problem of an elastic plate with discrete masses at the bottom edge was re-analyzed and the displacement results were identical in the z-direction and nearly identical in the x-direction. This indicates that moving the masses into the interior has no effect on the z-displacement and only a slight effect on the x-displacement at this analysis frequency (220 Hz), which is an expected result because this is a low-frequency example where the wavelengths of the forcing function are much larger than the thickness of the plate.

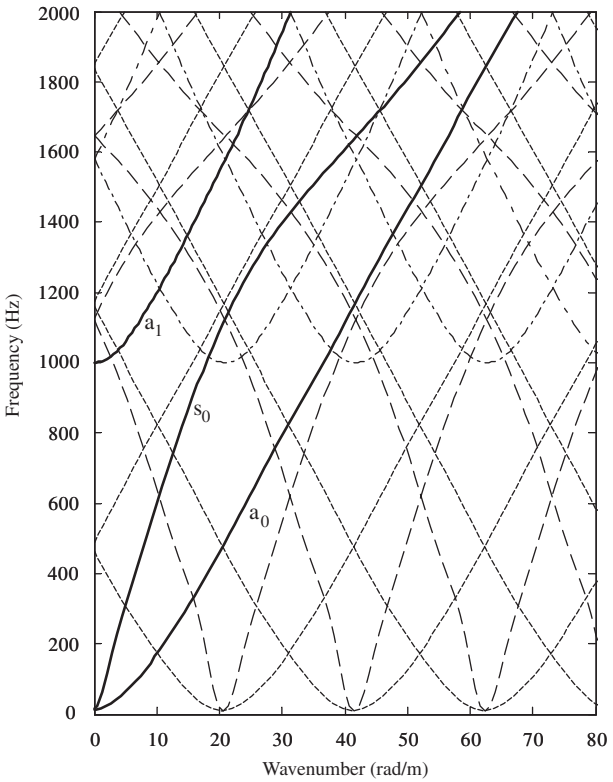

Fig. 6. Dispersion curve of plate with edge masses: (——) infinite plate waves, (·····) Floquet waves of the $n = 0$ antisymmetric wave (a_0), (– – – –) Floquet waves of the $n = 0$ symmetric wave (s_0), and (– · – · –) Floquet waves of the $n = 1$ antisymmetric wave (a_1).

4. Numerical example

A numerical example is now analyzed to show the dynamic response of elastic plates with masses on the edge and in the interior. This example was generated with the following system parameters: thickness is 0.1 m, density is 1200 kg/m^3, Lamé constant λ is 4.5×10^8 N/m^2, Lamé constant μ is 5.0×10^7 N/m^2, mass per unit length is 3.0 kg/m, and the mass separation distance is 0.3 m. Both elastic plate models were calculated using 15 modes ($-7\leqslant n\leqslant 7$) that produced a 60- $\times$ 60-element system matrix for the edge mass problem and a 120- $\times$ 120-element system matrix for the interior mass problem. For the interior mass problem, the masses were located at the mid-plane of the plate. The displacement values were output at location of 0.25 h (0.025 m) from the top of the plate. This problem is constructed so that the wavelengths of the shear and dilatational waves (0.204 and 0.677 m, respectively) were on the order of the length scales of the plate thickness and mass separation distance.

Fig. 6 is a plot of the dispersion curve for the plate with edge masses, which corresponds to free-wave propagation of the system. The figure was calculated by finding the location in the wavenumber–frequency plane where

$$\det[\mathbf{B}-\mathbf{V}]=0. \tag{68}$$

A frequency range of 0–2000 Hz was chosen so that the first three waves are present in the plot. Higher frequencies, where additional higher order modes exist, are not shown for plot clarity. The three solid lines represent locations of waves in the wavenumber–frequency plane that are present in the infinite plate without periodic masses, as well as the system with added masses. These waves are marked as follows: a_0 which is the zero-order antisymmetric wave, s_0 which is the zero-order symmetric wave, and a_1 which is the first-order

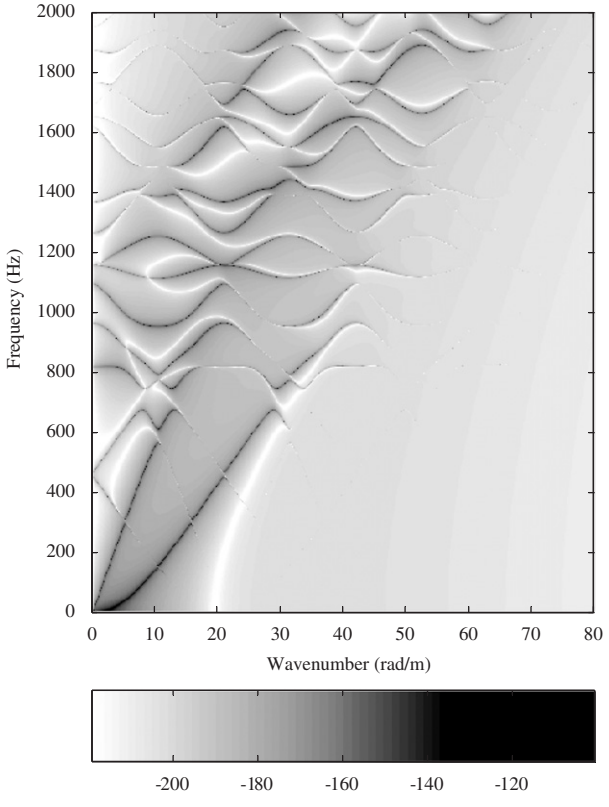

Fig. 7. Transfer function of tangential displacement divided by excitation force versus frequency and wavenumber for a plate with edge masses. Scale in dB ref m/Pa.

antisymmetric wave. The short dashed line is the Floquet waves associated with the $n = 0$ antisymmetric wave, the long dashed line is the Floquet waves associated with the $n = 0$ symmetric wave, and the short dashed–long dashed line is the Floquet waves associated with the $n = 1$ antisymmetric wave. These Floquet waves correspond to waves that share an integer multiple of a characteristic wavenumber of the infinite plate waves. This wavenumber is determined by

$$k_c = \frac{2\pi}{L} \tag{69}$$

and is equal to 20.9 rad/m. These Floquet waves represent energy that is propagating in the gaps between the periodic masses.

Figs. 7 and 8 present the transfer function of tangential displacement and normal displacement, respectively, divided by excitation force versus frequency and wavenumber for the plate with edge masses. In both figures, the data are displayed in the decibel scale referenced to meters per Pascal. The free wave that appears in the dispersion curve is clearly evident in both the tangential (Fig. 7) and normal (Fig. 8) displacement data. Figs. 9 and 10 present the transfer function between tangential displacement and the normal displacement, respectively, and force versus wavenumber at 900 Hz. Figs. 9 and 10 are divided into two plots for clarity: the upper plot is the problem of an elastic plate with edge masses and the lower plot is the elastic plate with interior masses. The dashed line in all four plots is the elastic plate solution with the absence of masses ($M = 0$).

Upon examination of Figs. 9 and 10, several features are noted. The resonance peaks are observable because the transfer function is no longer a smooth, continuous function of wavenumber and frequency, as the point masses and their characteristic length introduce additional resonances and anti-resonances into the response

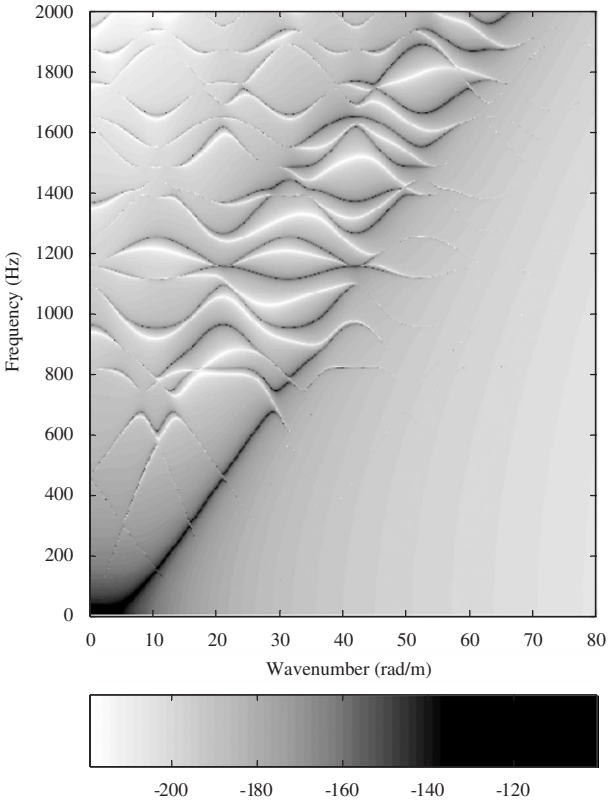

Fig. 8. Transfer function of normal displacement divided by excitation force versus frequency and wavenumber for a plate with edge masses. Scale in dB ref m/Pa.

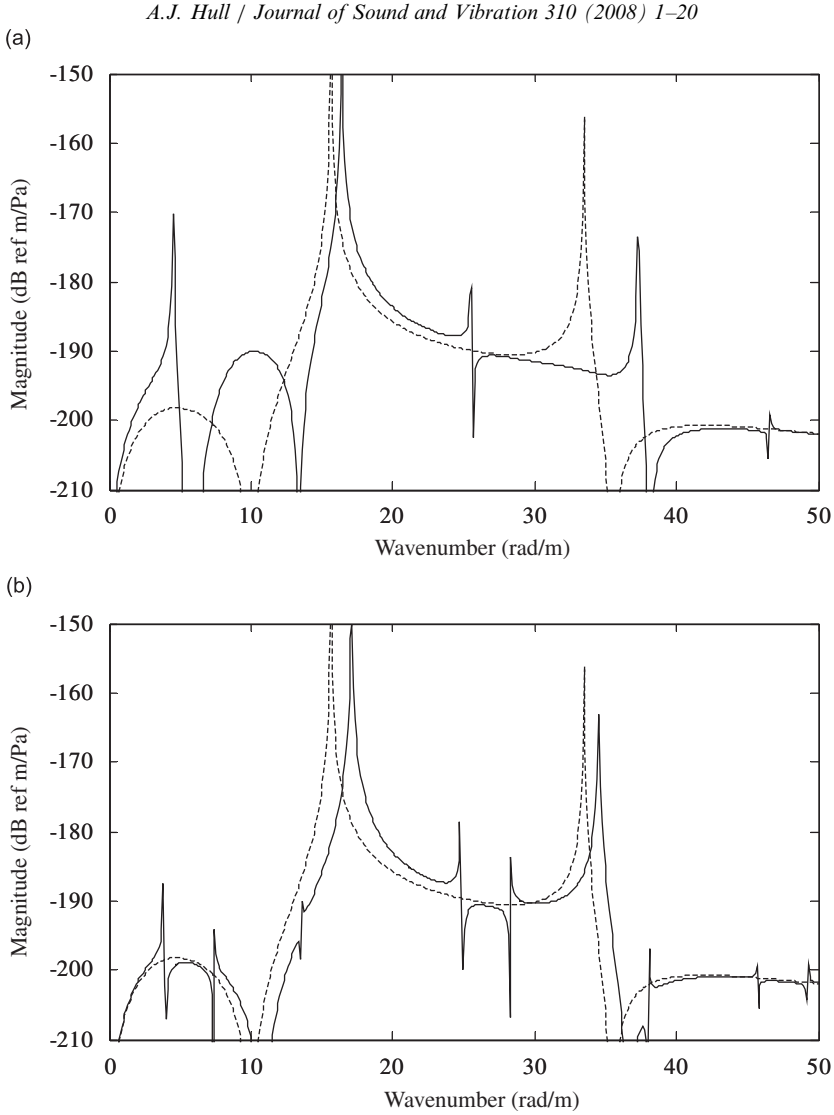

Fig. 9. Transfer function of tangential displacement divided by excitation force versus wavenumber at 900 Hz for (a) (_____) edge masses and (b) (_____) interior masses compared to (------) plate without masses.

of the system. This result is expected because the model has changed from a continuous, homogeneous infinite structure to a periodic structure that admits Floquet wave motion by the addition of discrete masses. Additionally, this effect has also been evident in previously developed low-frequency (bending-wave) models. The overall energy levels are approximately the same between the models with masses and the models without masses.

5. Conclusions

The solution of an elastic plate containing periodic edge and embedded masses harmonically loaded in space and time has been derived and found to compare favorably with previously developed thin plate models at low frequency. A numerical example of high-frequency dynamics was presented and the details discussed. The dispersion curve and transfer functions of tangential and normal displacements were illustrated. It was shown that the lower- and higher-frequency waves propagate at spatial lengths that correspond to integer multiples of the separation distance of the periodic masses. This characteristic makes the system become modally dense, even at low frequency and low wavenumber.

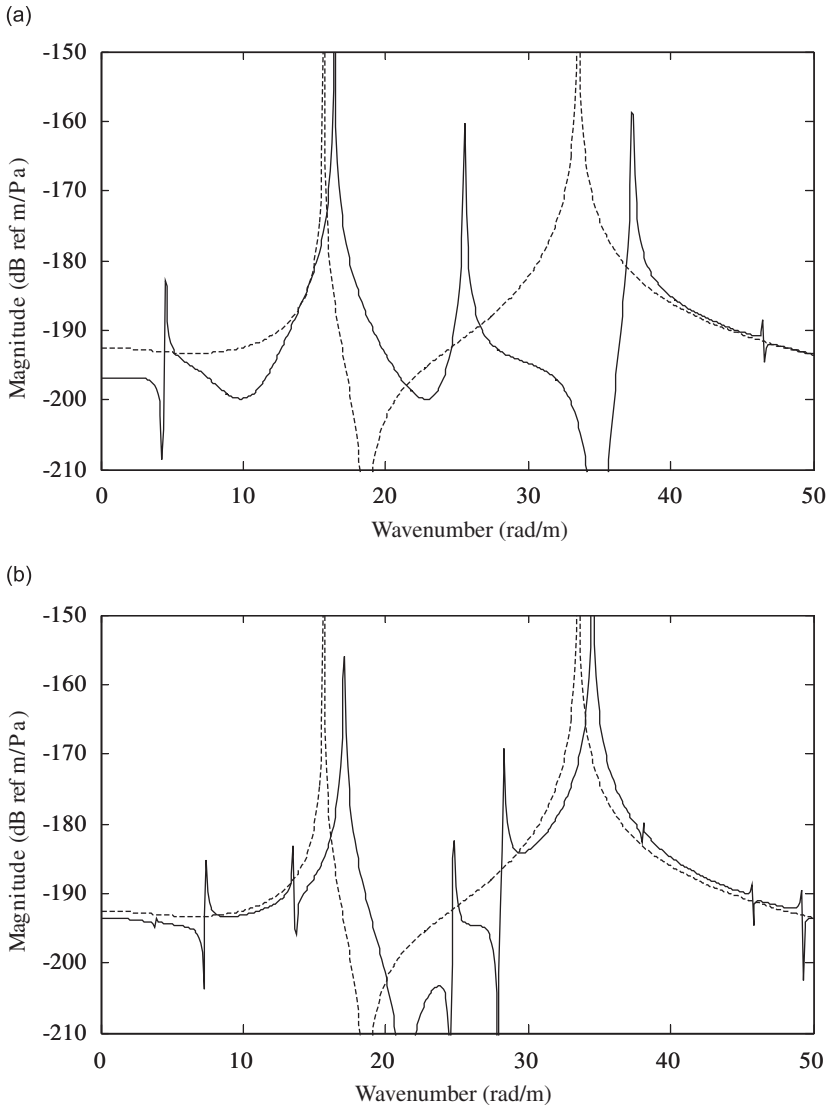

Fig. 10. Transfer function of normal displacement divided by excitation force versus wavenumber at 900 Hz for (a) (_____) edge masses and (b) (_____) interior masses compared to (------) plate without masses.

Acknowledgments

This work was funded by the Office of Naval Research. The author wishes to thank Anna Mastan for her help with the technical editing.

Appendix A. Matrix and vector entries

The entries of the matrixes and vectors in Eq. (37) are listed below. Without loss of generality, the bottom of the plate is defined as $z = a = 0$. For the $[\mathbf{A}^{(n)}(k_n)]$ matrix, the nonzero entries are

$$a_{11} = (-\alpha_n^2\lambda - 2\alpha_n^2\mu - \lambda k_n^2)\sin(\alpha_n h), \tag{A.1}$$

$$a_{12} = (-\alpha_n^2\lambda - 2\alpha_n^2\mu - \lambda k_n^2)\cos(\alpha_n h), \tag{A.2}$$

$$a_{13} = 2i\mu k_n \beta_n \cos(\beta_n h) \tag{A.3}$$

$$a_{14} = -2i\mu k_n \beta_n \sin(\beta_n h), \tag{A.4}$$

$$a_{21} = 2i\mu k_n \alpha_n \cos(\alpha_n h), \tag{A.5}$$

$$a_{22} = -2i\mu k_n \alpha_n \sin(\alpha_n h), \tag{A.6}$$

$$a_{23} = \mu(\beta_n^2 - k_n^2)\sin(\beta_n h), \tag{A.7}$$

$$a_{24} = \mu(\beta_n^2 - k_n^2)\cos(\beta_n h), \tag{A.8}$$

$$a_{32} = -\alpha_n^2 \lambda - 2\alpha_n^2 \mu - \lambda k_n^2, \tag{A.9}$$

$$a_{33} = 2i\mu k_n \beta_n, \tag{A.10}$$

$$a_{41} = 2i\mu k_n \alpha_n, \tag{A.11}$$

and

$$a_{44} = \mu(\beta_n^2 - k_n^2). \tag{A.12}$$

For the $[\mathbf{U}^{(n)}(k_n)]$ matrix, the nonzero entries are

$$u_{31} = \frac{-M\omega^2}{L}\alpha_n, \tag{A.13}$$

$$u_{34} = \frac{-M\omega^2}{L} i k_n, \tag{A.14}$$

$$u_{42} = \frac{-M\omega^2}{L} i k_n, \tag{A.15}$$

and

$$u_{43} = \frac{M\omega^2}{L}\beta_n. \tag{A.16}$$

The $\{\mathbf{x}^{(0)}(k)\}$ vector entries are

$$\{\mathbf{x}^{(0)}(k)\} = \{\, A \quad B \quad C \quad D \,\}^{\mathrm{T}} \equiv \{\, A_0 \quad B_0 \quad C_0 \quad D_0 \,\}^{\mathrm{T}}. \tag{A.17}$$

The $\mathbf{x}$ vector entries are

$$\mathbf{x} = \{\, \ldots \quad A_{-1} \quad B_{-1} \quad C_{-1} \quad D_{-1} \quad A_0 \quad B_0 \quad C_0 \quad D_0 \quad A_1 \quad B_1 \quad C_1 \quad D_1 \quad \ldots \,\}^{\mathrm{T}}. \tag{A.18}$$

The $\mathbf{f}$ vector entries are

$$\mathbf{f} = \{\, -F \quad 0 \quad 0 \quad 0 \,\}^{\mathrm{T}}. \tag{A.19}$$

The entries of the matrixes in Eq. (66) are listed below. Without loss of generality, the location of the masses in the z-direction is defined as $z = b = 0$. For the $[\mathbf{B}^{(n)}(k_n)]$ matrix, the nonzero entries are

$$b_{11} = (-\alpha_n^2 \lambda - 2\alpha_n^2 \mu - \lambda k_n^2)\sin(\alpha_n c), \tag{A.20}$$

$$b_{12} = (-\alpha_n^2 \lambda - 2\alpha_n^2 \mu - \lambda k_n^2)\cos(\alpha_n c), \tag{A.21}$$

$$b_{13} = 2i\mu k_n \beta_n \cos(\beta_n c), \tag{A.22}$$

$$b_{14} = -2i\mu k_n \beta_n \sin(\beta_n c), \tag{A.23}$$

$$b_{21} = 2i\mu k_n \alpha_n \cos(\alpha_n c), \tag{A.24}$$

$$b_{22} = -2i\mu k_n \alpha_n \sin(\alpha_n c), \tag{A.25}$$

$$b_{23} = \mu(\beta_n^2 - k_n^2)\sin(\beta_n c), \tag{A.26}$$

$$b_{24} = \mu(\beta_n^2 - k_n^2)\cos(\beta_n c), \tag{A.27}$$

$$b_{32} = -\alpha_n^2\lambda - 2\alpha_n^2\mu - \lambda k_n^2, \tag{A.28}$$

$$b_{33} = 2i\mu k_n \beta_n, \tag{A.29}$$

$$b_{36} = \alpha_n^2\lambda + 2\alpha_n^2\mu + \lambda k_n^2, \tag{A.30}$$

$$b_{37} = -2i\mu k_n \beta_n, \tag{A.31}$$

$$b_{41} = 2i\mu k_n \alpha_n, \tag{A.32}$$

$$b_{44} = \mu(\beta_n^2 - k_n^2), \tag{A.33}$$

$$b_{45} = -2i\mu k_n \alpha_n, \tag{A.34}$$

$$b_{48} = -\mu(\beta_n^2 - k_n^2), \tag{A.35}$$

$$b_{51} = \alpha_n, \tag{A.36}$$

$$b_{54} = ik_n, \tag{A.37}$$

$$b_{55} = -\alpha_n, \tag{A.38}$$

$$b_{58} = -ik_n, \tag{A.39}$$

$$b_{62} = ik_n, \tag{A.40}$$

$$b_{63} = -\beta_n \tag{A.41}$$

$$b_{66} = -ik_n, \tag{A.42}$$

$$b_{67} = \beta_n, \tag{A.43}$$

$$b_{75} = (-\alpha_n^2\lambda - 2\alpha_n^2\mu - \lambda k_n^2)\sin(\alpha_n a), \tag{A.44}$$

$$b_{76} = (-\alpha_n^2\lambda - 2\alpha_n^2\mu - \lambda k_n^2)\cos(\alpha_n a), \tag{A.45}$$

$$b_{77} = 2i\mu k_n \beta_n \cos(\beta_n a), \tag{A.46}$$

$$b_{78} = -2i\mu k_n \beta_n \sin(\beta_n a), \tag{A.47}$$

$$b_{85} = 2i\mu k_n \alpha_n \cos(\alpha_n a), \tag{A.48}$$

$$b_{86} = -2i\mu k_n \alpha_n \sin(\alpha_n a), \tag{A.49}$$

$$b_{87} = \mu(\beta_n^2 - k_n^2)\sin(\beta_n a), \tag{A.50}$$

and

$$b_{88} = \mu(\beta_n^2 - k_n^2)\cos(\beta_n a). \tag{A.51}$$

The $[\mathbf{V}^{(n)}(k_n)]$ matrix can be written as

$$\mathbf{V}^{(n)}(k_n) = \begin{bmatrix} \mathbf{U}^{(n)}(k_n) & \mathbf{0} \\ \mathbf{0} & \mathbf{0} \end{bmatrix}, \tag{A.52}$$

where $[\mathbf{U}^{(n)}(k_n)]$ is defined in Eqs. (A.13)–(A.16) and $\mathbf{0}$ is a four by four matrix whose entries are all zero. The $\{\mathbf{y}^{(0)}(k)\}$ vector entries are

$$\begin{aligned} \{\mathbf{y}^{(0)}(k)\} &= \{\, A \quad B \quad C \quad D \quad E \quad F \quad G \quad H \,\}^{\mathrm{T}} \\ &\equiv \{\, A_0 \quad B_0 \quad C_0 \quad D_0 \quad E_0 \quad F_0 \quad G_0 \quad H_0 \,\}^{\mathrm{T}}. \end{aligned} \tag{A.53}$$

The $\mathbf{y}$ vector entries are

$$\begin{aligned} \mathbf{y} = \{ \cdots \quad & A_{-1} \quad B_{-1} \quad C_{-1} \quad D_{-1} \quad E_{-1} \quad F_{-1} \quad G_{-1} \quad H_{-1} \\ & A_0 \quad B_0 \quad C_0 \quad D_0 \quad E_0 \quad F_0 \quad G_0 \quad H_0 \\ & A_1 \quad B_1 \quad C_1 \quad D_1 \quad E_1 \quad F_1 \quad G_1 \quad H_1 \quad \cdots \}^{\mathrm{T}}. \end{aligned} \tag{A.54}$$

The $\mathbf{h}$ vector entries are

$$\mathbf{h} = \{\, -F \quad 0 \quad 0 \quad 0 \quad 0 \quad 0 \quad 0 \quad 0 \,\}^{\mathrm{T}}. \tag{A.55}$$

References

[1] K.F. Graff, *Wave Motion in Elastic Solids*, Dover Publications, New York, 1975.

[2] R.D. Mindlin, Influence of rotary inertia and shear on flexural motions of isotropic elastic plates, *Journal of Applied Mechanics* 18 (1951) 31–38.

[3] H. Lamb, On waves in an elastic plate, *Proceedings of the Royal Society of London Series A* 93 (1917) 114–120.

[4] M.F.M. Osborne, S.D. Hart, Transmission, reflection, and guiding of an exponential pulse by a steel plate in water, I: theory, *Journal of the Acoustical Society of America* 17 (1) (1945) 1–18.

[5] D.G. Crighton, The free and forced waves on a fluid-loaded elastic plate, *Journal of Sound and Vibration* 63 (2) (1979) 225–235.

[6] A. Freedman, The variation, with the Poisson ratio, of Lamb modes in a free plate, I: general spectra, *Journal of Sound and Vibration* 137 (2) (1990) 209–230.

[7] A. Freedman, The variation, with the Poisson ratio, of lamb modes in a free plate, II: at transitions and coincidence values, *Journal of Sound and Vibration* 137 (2) (1990) 231–247.

[8] J. Dickey, G. Maidanik, H. Überall, The splitting of dispersion curves for the fluid-loaded plate, *Journal of the Acoustical Society of America* 98 (4) (1995) 2365–2367.

[9] A. Freedman, Effects of fluid loading on lamb mode spectra, *Journal of the Acoustical Society of America* 99 (6) (1996) 3488–3496.

[10] A. Freedman, The variation, with the Poisson ratio, of Lamb modes in a free plate, III: behaviour of individual modes, *Journal of Sound and Vibration* 137 (2) (1990) 249–266.

[11] A.J. Hull, Analysis of a fluid-loaded thick plate, *Journal of Sound and Vibration* 279 (1–2) (2005) 497–507.

[12] B.R. Mace, Sound radiation from a plate reinforced by two sets of parallel stiffeners, *Journal of Sound and Vibration* 71 (3) (1980) 435–441.

[13] D.J. Mead, K.K. Pujara, Space-harmonic analysis of periodically supported beams: response to convected random loading, *Journal of Sound and Vibration* 14 (4) (1971) 525–541.

[14] B.R. Mace, Periodically stiffened fluid-loaded plates, I: response to convected harmonic pressure and free wave propagation, *Journal of Sound and Vibration* 73 (4) (1980) 473–486.

[15] B.R. Mace, Periodically stiffened fluid-loaded plates, II: response to line and point forces, *Journal of Sound and Vibration* 73 (4) (1980) 487–504.

[16] G.P. Eatwell, D. Butler, The response of a fluid-loaded, beam-stiffened plate, *Journal of Sound and Vibration* 84 (3) (1982) 371–388.

[17] G.P. Eatwell, Free-wave propagation in an irregularly stiffened, fluid-loaded plate, *Journal of Sound and Vibration* 88 (4) (1983) 507–522.

[18] B.A. Cray, Acoustic radiation from periodic and sectionally aperiodic rib-stiffened plates, *Journal of the Acoustical Society of America* 95 (1) (1994) 256–264.

[19] J.W. Nicholson, L.A. Bergman, Vibration of thick plates carrying concentrated masses, *Journal of Sound and Vibration* 103 (3) (1985) 357–369.

[20] G.S. Palani, N.R. Iyer, T.V.S.R. Appa Rao, An efficient finite element model for static and vibration analysis of plates with arbitrarily located eccentric stiffeners, *Journal of Sound and Vibration* 166 (3) (1993) 409–427.

[21] S.P. Timoshenko, J.N. Goodier, *Theory of Elasticity*, McGraw-Hill, New York, 1934.